Solid-State Electronics 77 (2012) 93–100

Contents lists available at SciVerse ScienceDirect

Solid-State Electronics

journal homepage: www.elsevier.com/locate/sse

Wireless powering electronics and spiral coils for implant microsystem toward nanomedicine diagnosis and therapy in free-behavior animal

Chih-Wei Chang [a], Kuan-Chou Hou [a], Li-Jung Shieh [a], Sheng-Hsin Hung [a], Jin-Chern Chiou [a,b,*]

[a] Department of Electrical Engineering, National Chiao-Tung University, No. 1001, University Road, Hsinchu City 30010, Taiwan
[b] China Medical University, No. 91, Hsueh-Shih Road, Taichung City 40402, Taiwan

ARTICLE INFO

Article history:
Available online 29 June 2012

Keywords:
Wireless powering
Batteryless microsystem
Coil antenna
Low dropout regulator

ABSTRACT

In this paper, we present a wireless RF-powering electronics system approach for batteryless implantable biomedical microsystem with versatile sensors/actuators on laboratory animals toward diagnosis and therapy applications. Miniaturized spiral coils as a wireless power module with low-dropout (LDO) linear regulator circuit convert RF signal into DC voltage, provide a batteryless implantation for truly free-behavior monitoring without wire dragging. Presented design achieves low quiescent-current and Line/Load Regulation, high antenna/current efficiency with safety considerations including temperature and electromagnetic absorption issues to avoid damage to the implanted target volume of tissue. Related system performance measurements have been successfully completed to demonstrate the wireless powering capabilities in desired implantable microsystems.

1. Introduction

Neuroscience engineering together with in vivo real time biomedical information, such as neural activity, recorded by implant neural sensors and microsystems is ultimately crucial for nanomedicine and bio-logical researches to identify and develop treatments for brain disorders i.e. epilepsy. For such applications in animal model studies, microsystems that consist of neural sensors, amplifiers, data converters/operators and data transmission units are used to capture neural information from animals and transfer the data to a laptop for further analysis.

Generally, at least two types of wire connection are required for powering and data transmission. Use of wire connection between animal and instrumentations can cause serious problem even lead to the death of implanted animal when wire drag happens. Swivels are sometimes used to solve the dragging, but the price can be another problem, the channel numbers are limited and the implanted laboratory animal still cannot behave in their nature condition because the wires. Benefit to the rapid developments of wireless communication, many different kind of wireless solution, including Zigbee [1] and Bluetooth [2], have been commercialized and applied in animal studies. Batteries are common used to eliminate the problem of power wires. However, batteries dominate the size and the cost of the implant device and become less attractive when the implant devices get smaller and need to replace their batteries occasionally [3]. Therefore, the demand for developing continuous monitoring in long-term, real-time prosthetics in free-behavior implanted animal is restricted by the capacity of the battery. A biomedical system constructed by bio-potential sensors [4] and actuators with miniaturized powering device receiving RF-power from an external host is then highly desirable.

Currently, there are various methods for wireless transfer of power to biomedical microsystems, including ultrasonic energy transmission [5], capacitive coupling [6] and inductive coupling. Ultrasonic energy harvest systems transfer the mechanical energy into the implant device through skin, but suffer from low energy conversion capability [7]. Capacitive coupling declares clean and quiet telemetry by using metal plates and skin tissue as capacitors [6], however, it can never be applied in animals that need to be monitored under freely moving status. Comparing to other two method, inductive link achieves more possibility to transfer energy through an open air field with reasonable transmission efficiency.

In this paper, we present an inductive coupled wireless powering system which contains inductive coils and low-dropout regulator design for implant microsystem toward free-behavior animal applications. Section 2 describes the overall wireless powering structure in an implantable microsystem. The development of the inductive coupling coils and low dropout regulator is detailed in Sections 3 and 4, following with performance test of the proposed wireless powering system in Section 5. Section 6 summarizes this paper with a brief conclusion.

* Corresponding author at: Department of Electrical Engineering, National Chiao-Tung University, No. 1001, University Road, Hsinchu City 30010, Taiwan. Tel.: +886 3 5712121x31881; fax: +886 5 5715998.
E-mail addresses: chihwei@nctu.edu.tw (C.-W. Chang), hiho.ece94g@nctu.edu.tw (K.-C. Hou), ljs.ece93g@nctu.edu.tw (L.-J. Shieh), sean_hung@analog.com.tw (S.-H. Hung), chiou@mail.nctu.edu.tw (J.-C. Chiou).

0038-1101/$ - see front matter © 2012 Elsevier Ltd. All rights reserved.
http://dx.doi.org/10.1016/j.sse.2012.05.020

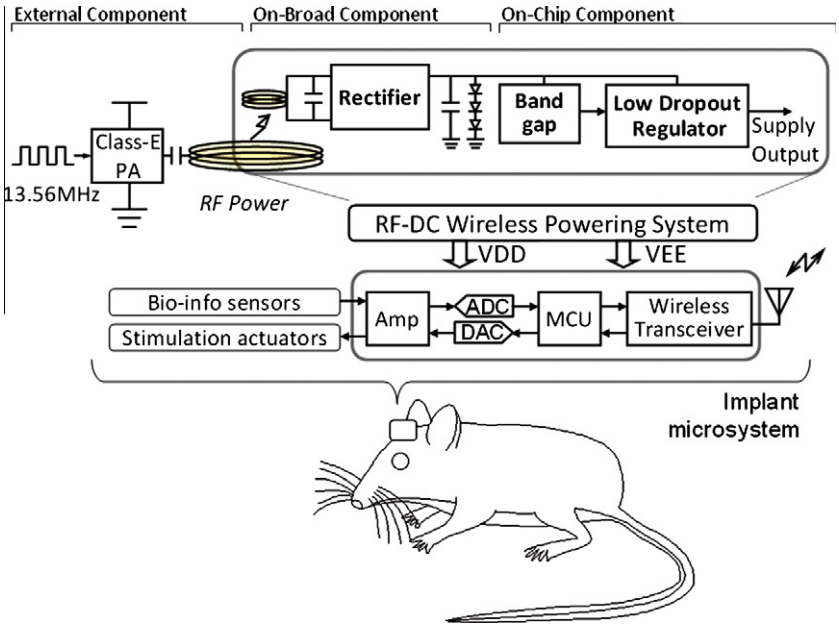

Fig. 1. Schematic diagram of the proposed RF–DC wireless powering system which receives RF power from an external PA and provides system supplies to a conceptual implant microsystem.

2. Wireless powering system structure

Fig. 1 displays the block diagram of microsystem with bio-sensors i.e. ExG, chemical or temperature sensors, and stimulation actuators i.e. drag delivery for nanomedicine diagnosis and therapy. Wireless transceiver in the microsystem transmits bio-info data to and receives commands from an external host, while proposed RF–DC wireless powering system receives RF power from an external host and provides system supplies to the implant microsystem. The RF power produced by a Class-E amplifier is coupled into the receiving coil via a tuned LC network followed by a full-wave rectifier and low dropout (LDO) regulators to produce stable system supplies [8]. The proposed wireless powering system can serve as an additional small module to be applied to different microsystems. The schematic of wireless powering system can also be observed in Fig. 1. External component includes PA and RF power transmission coil, on-broad components involves receive coil, rectifier, smoothing capacitance and bias diode, and the on-chip component includes LDO regulator with band gap bias circuit and thermal protection circuitry.

In the inductive coupled power transmission design, the main contribution to the power loss is the electromagnetic wave reflection at the air-skin interface and heat dissipation effect inside the tissues [9]. Also, reliable transmission efficiency with enough transmission distance becomes one of the considerations. Low RF powering frequency provides longer transmission distance but also makes receiver coil bigger. Furthermore, electromagnetic wave shows its absorption and reflection property by the skin tissue when frequency range is approximately higher 20 MHz and lower than 1 MHz, respectively. In this paper, 13.56 MHz radio frequency is chosen because it is one of the ISM band and its low tissue absorbability to avoid damage on animal tissue.

3. Inductive coupling spiral coils theory and design

3.1. Inductive link theory and design procedure

The radio frequency power is transmitted through coupled coils, which follows the electromagnetic induction of Faraday's Law. Various approaches have been presented for inductive link optimization in implantable electronics [10–12]. Fig. 2 illustrates a simplified inductive powering model [13,14]. L_1 is the primary coil driven by an ac source Vs, which is often an efficient class-E power amplifier. L_2, is the secondary coil that is integrated with the implant electronics. M is the mutual inductance between two coils. Coil windings have parasitic resistance and capacitance associated with them, which are represented by lumped elements R_{s1} and R_{s2}. Capacitors C_{s1} and C_2 are added to form a pair of resonant LC-tank with L_1 and L_2, respectively.

Magnetic flux lines are formed around the primary coil as a result of the flow of current though it and the voltage induced in the secondary coil is due to the magnetic flux passing though. The equivalent resistance R_e, reflected back into the primary coil can be expressed as:

$$R_e = \frac{(\omega M)^2}{R_{s2}R_L} = \frac{R_{AC}K^2Q_1Q_2}{R_{AC} + Q_2^2R_{s2}} \times R_{s1} \tag{1}$$

where K, Q_1 and Q_2 are the coupling coefficient and unloaded quality factor of the two coils. The mutual inductance of two aligned coils that having diameters r_1 and r_2, turns N_1 and N_2 and separated by distance x is given by the following expression [15]:

$$M = \frac{\mu_0 N_1 r_1^2 N_2 r_2^2 \pi}{2\sqrt{(r_2^2 + x^2)^3}} \tag{2}$$

where $\mu_0 = 4\pi \times 10^{-9}$ H/cm. And the optimal transmission efficiency is readily found in the literature [16]:

$$\eta_{OPT} = \frac{K^2Q_1Q_2}{[1 + (1 + K^2Q_1Q_2)^{1/2}]^2} \tag{3}$$

The shared magnetic flux between coils results in a coupling coefficient K, where $0 < K < 1$, is given by:

$$K = \frac{M}{\sqrt{L_1L_2}} \tag{4}$$

The coupling coefficient K is only determined by the coil dimension (diameter and distance), and the quality factor is defined by the coil structure and material. The related equation concludes that optimum powering efficiency increases as $k^2Q_1Q_2$ increases [17]. For high quality factor, low skin-effect, low resistance wires and

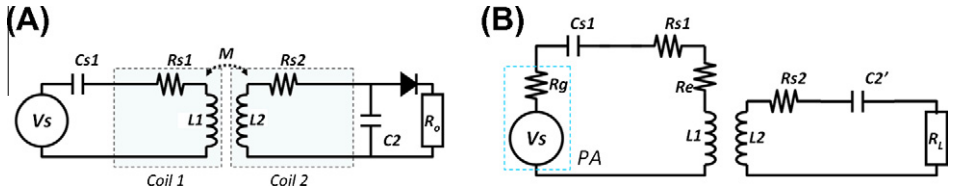

Fig. 2. (A) Inductive powering circuit model. (B) Equivalent circuit.

Fig. 3. Fabricated receiving and external coils.

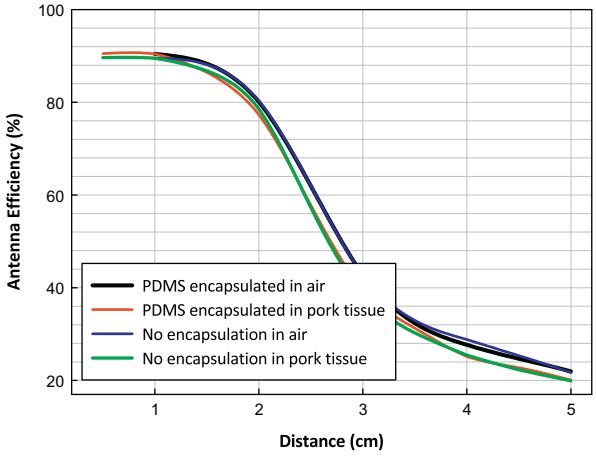

Fig. 4. Antenna efficiency characterization with PDMS encapsulation under conditions in air and tissue (pork).

single layer spiral coil structure were utilized in this work. Also, to maximize the coupling coefficient K, optimal values of geometry of the coils are obtained according to the expressions in [16]. Calculate R_{S2} and R_{S1} from desired rectifier performance and powering specification. Therefore, L_1 and L_2 can be designed and obtained and realized by experimental measurements. Then, the resonance capacitance C_{S1} and C_2 can be found according to desired transmission frequency.

3.2. Fabricated results and measurements

Fig. 3 shows the optical photographs of the fabricated receiving and external coils made by 24/16 AWG cupper wire with 1.5 cm and 4 cm in diameter. The inductance, parasitic resistance, parasitic capacitance and resonate capacitance of the transmission coil are 15 μH, 11.5 Ω, 2.73 pF and 6.4 pF, while the receive coil exhibits 521 nH, 16.7 Ω, 3.71 pF and 260.7 pF, respectively. The antenna

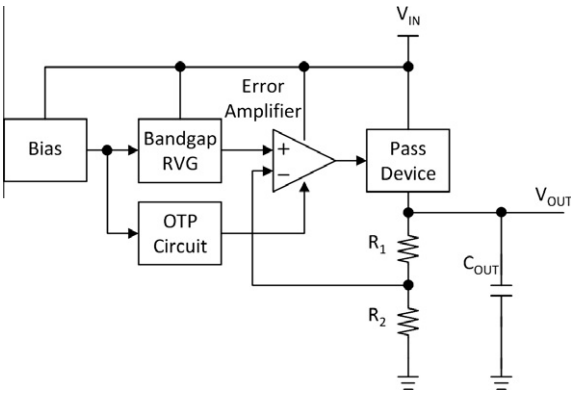

Fig. 5. Block diagram of the proposed low-dropout linear regulator.

efficiency is characterized with PDMS coating as bio-protection in implanted tissue. Measurement result under conditions in air/tissue (pork) and with/without PDMS encapsulation is illustrated in Fig. 4, which results no obvious influence from packaging.

4. Low dropout regulator design

4.1. Circuit design

Fig. 5 illustrates the block diagram of the proposed low-dropout linear regulator. The architecture is modified from a typical low-dropout regulator topology [18] with power MOSFET and thermal protection unit to enhance the driving current and avoid temperature damage on tissue. The error amplifier amplifies the voltage difference between the reference voltage and divided load voltage and switches the power MOSFET (PMOS). Output voltage is described as:

$$V_{OUT} = V_{REF}\left(\frac{R_1 + R_2}{R_2}\right) \tag{5}$$

Another design issue in the linear regulator is the stability problem. According to bode plot analysis, the output capacitance and its equivalent series resistance (ESR) decides the zero point to increase the phase margin. However, the ESR must be carefully designed in appropriate range to ensure the system stability.

Fig. 6 shows the circuit schematic of the error amplifier. M_{I27} is the power MOSFET illustrated in Fig. 5. Also, stability is one of the design key points. In this design, ceramic capacitance with low ESR is used as output capacitance, which can cause low phase margin and lead into un-stable condition. Therefore, extra RC-compensation is introduced to enhance the system stability. In Fig. 6, current limitation control by two Poly resistances which is inverse proportional to current. PIP capacitance I48 and resistor R_{I31} are used for Miller compensation. PIP capacitance M_{I44} and M_{I39} are used as internal smoothing capacitances for spike rejection. MOS M_{I3} acts as output switch, which controlled by thermal protection circuit.

Fig. 7A shows the detailed schematic of a temperature-independent bandgap reference voltage generator (RVG) [19]. In Fig. 7A,

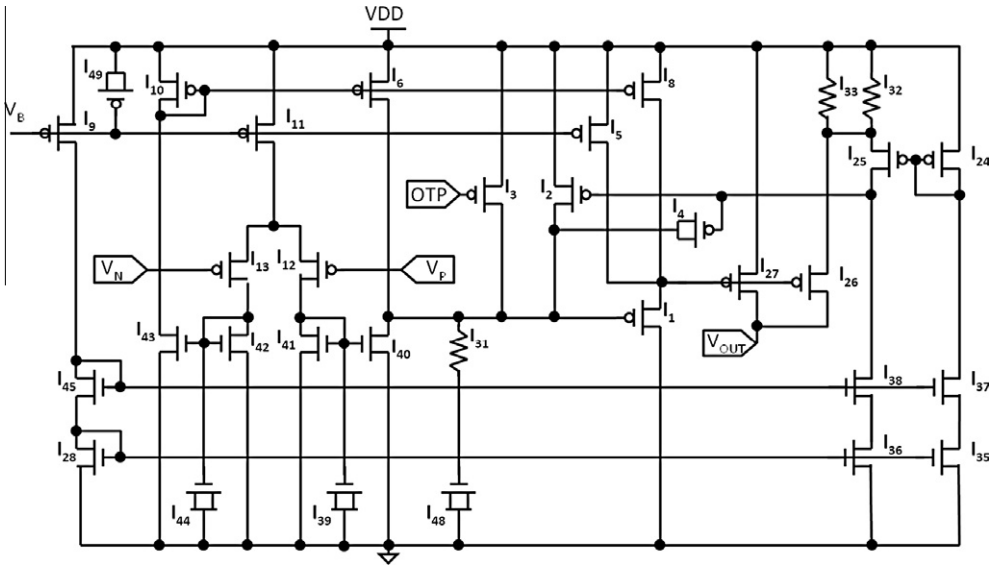

Fig. 6. Error amplifier circuit.

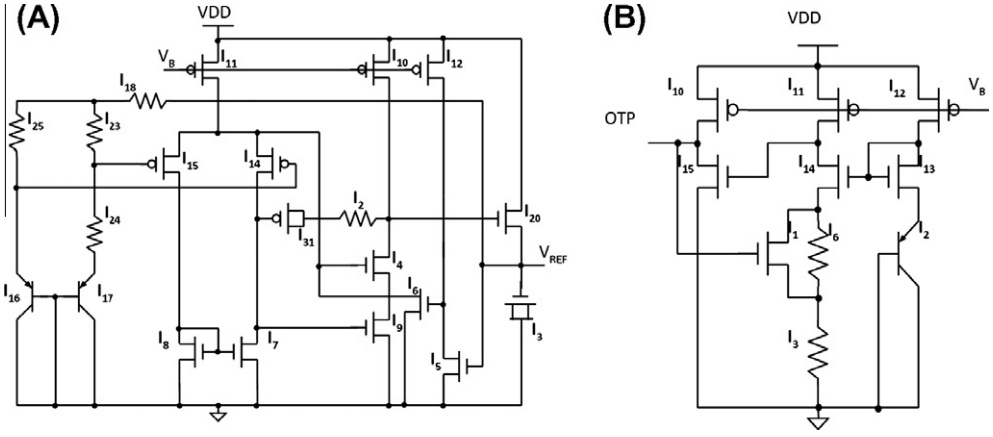

Fig. 7. (A) Bandgap voltage reference generator and (B) over-thermal protection circuit.

the PNP BJT Q_{I16} and Q_{I17} act as negative- and positive-TC voltage devices produce a temperature independent voltage difference to the operational amplifier. A resistor R_{I18} is used to adjust the output VREF. PIP capacitance M_{I31} and resistor R_{I2} are used for Miller compensation. M_{I5} and M_{I6} act as a startup for quicker response. M_{I4} is an extra gain stage for higher PSRR. M_{I20} is used for extra ESD protection, while the PIP capacitance M_{I3} used as a filter and bias. Fig. 7B illustrates the thermal protection circuit schematic. The over-temperature protection (OTP) design is used to avoid thermal damage on tissue due to the high temperature (>40 °C) caused by the operating circuit. In Fig. 7B, R_{I3} is a ROND resistor in tsmc 0.35 μm process, which has high temperature coefficient (PTC1 = 1.51e − 3). When T raise, voltage drop on R_{I3} increase, then turn-on M_{I14}, increase current flow passing MI_{14}, turn-on MI_{15}, pull down OTP. Hysteresis functions when temperature drop down lower than 40 °C, M_{I14} will not off immediately due to the current provided by BJT Q_{I2}. Until the temperature is lower enough, say <37 °C, voltage drop on R_{I3} decrease, current decrease, M_{I14} turn-off, M_{I15} off, OTP pull high.

4.2. Fabricated results and measurements

The LDO regulator chip is fabricated via TSMC 0.35um 2P4 M process. The die size is 1.42 × 0.95 mm2. Fig. 8A shows the optical microphotograph. Fig. 8B is the test result of the power supply rejection ratio. The measured PSRR is around 70.883 dB and 0.165 dB at 10 kHz and 13.56 MHz, respectively. Comparing to the simulation result of PSRR (~81.44 dB), the main difference is that simulation consists of only pure capacitance, but in practice, parasitic inductance does exist in the output ceramic capacitance, which decreases the high frequency performance in PSRR.

The stability test of the LDO regulator displays the ripple and noise on the output voltage level under different current loading. Fig. 9A output stability observation under I_{OUT} = 200 mA. Result shows that the maximal noise level is lower than 3–4 mV. Low ripple and noise performance is one of the great property of linear regulator. Fig. 9B present the output ripple caused by a current loading from 0 mA to 200 mA. Output transient behaves a 308–264 mV spike, say 17–14% variance in output voltage, under the condition V_{IN} from 3 V to 6 V, respectively. The output transient performance can be easily improved by increase the quiescent current but also increase the power consumption. Fig. 9C illustrates the output ripple observation under a sudden maximal current loading. The maximal output current varies under different V_{IN} condition. Result shows that the peak of the spike is less than 300 mV. Line transient is the output current ripple caused by the input voltage variance. Fig. 9D shows the spike observation under loading current 200 mA with V_{IN} variance from 2.6 V to 6 V. The

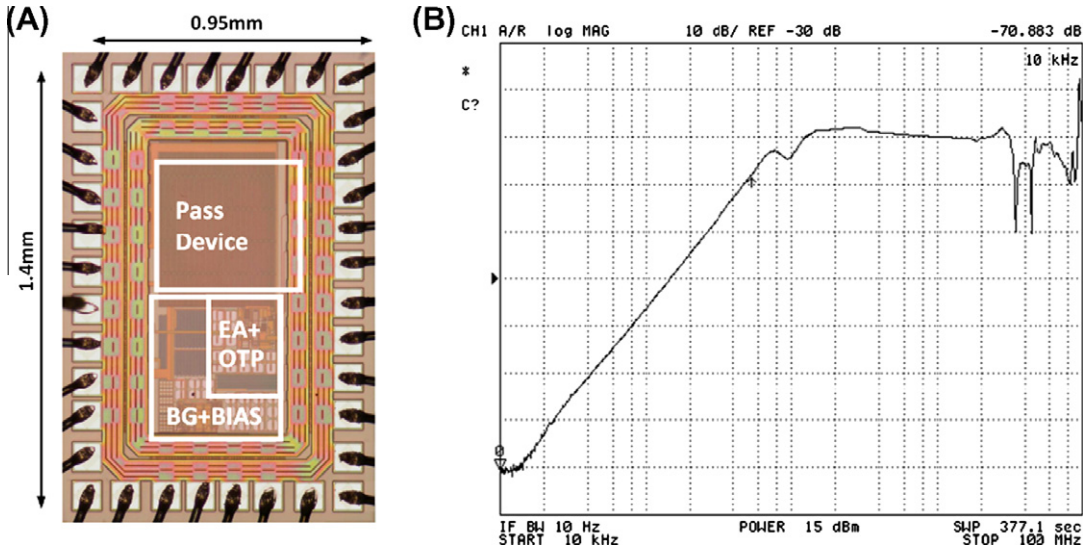

Fig. 8. (A) Optical microphotograph of the fabricated chip (B) PSRR.

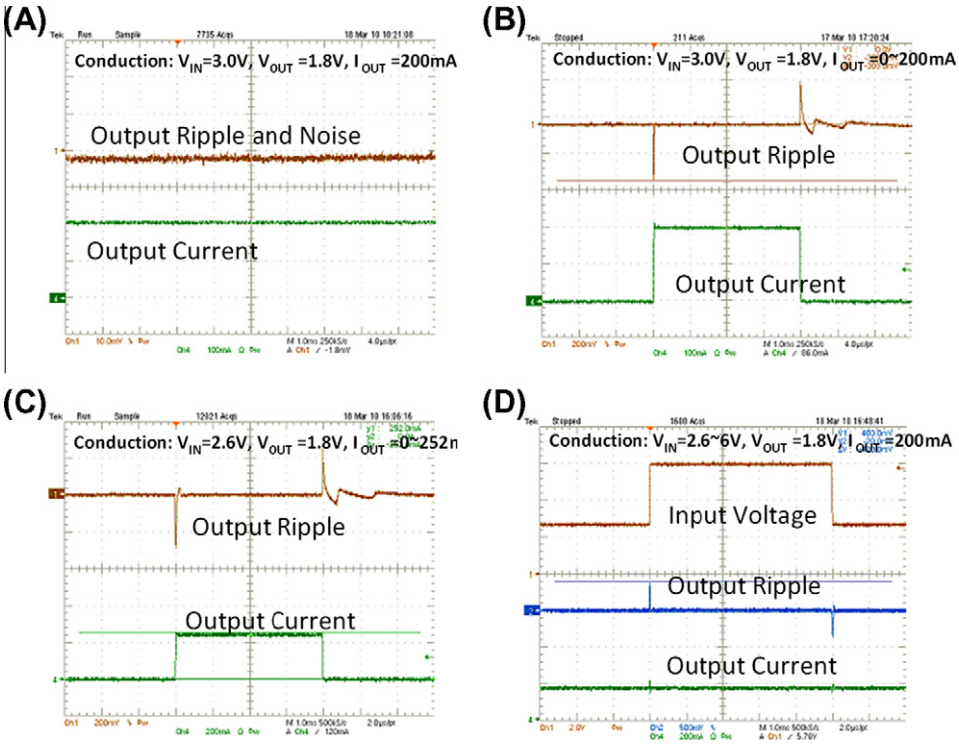

Fig. 9. (A) Stability test @ I_{OUT} = 200 mA (B) load transient test I_{OUT} = 0–200 mA @ V_{IN} = 3 V (C) ripple observation @ load 0–252 mA (D) output spike @ V_{IN} = 2.6–6 V.

overall Line Regulation performance is between 1.5 and 4.5 mV, cause 0.0833–0.25% variance in output current.

Table 1 shows the measured Load/Line Regulation Result. Note that when the I_{OUT} = 200 mA under V_{IN} from 5 V to 6 V, the system is thermal shutdown due to the over thermal protection (OTP). Generally speaking, the Load Regulation is between 0.5 and 5 mV, which is around 0.0278–0.278% variance in output voltage. Table 2 summarizes the measured performance of the presented LDO regulator comparing to other works.

Presented chip shows low drop out voltage, wide input range with reasonable quiescent current. Additionally, thermal-protection (<40 °C) design is also included in the present linear regulator to avoid damage in implanted target for implant device applications. Some equations used for specification comparison are listed below:

$$V_{Drop} = V_{in} - V_{OUT} \ @ \ I_{OUT\ MAX} \tag{6}$$

$$I_{eff} = \frac{I_{OUT\_MAX}}{I_{IN\_MAX} + I_Q} \tag{7}$$

5. Wireless powering system performance

After the fabrication of spiral coils and LDO regulator chip, PCB level integration is utilized for system performance characteriza-

Table 1
Load/Line Regulation Test Result.

	V_{IN} (V)	2.6	3.3	4.2	5.0	6.0	Line Regulation
I_{OUT} = 0 mA	V_{OUT} (V)	1.828	1.8285	1.829	1.8295	1.8285	1.5 mV
I_{OUT} = 50 mA		1.828	1.829	1.83	1.8305	1.8305	2.5 mV
I_{OUT} = 100 mA		1.828	1.83	1.831	1.8325	1.8325	4.5 mV
I_{OUT} = 200 mA		1.8285	1.8315	1.834	OTP	OTP	NA
	Load Regulation	0.5 mV	3 mV	5 mV	NA	NA	

Table 2
Summary of LDO regulator performance.

	[20]	[21]	[22]	This work
Year	2006	2008	2010	2011
Technology (μm)	0.13	0.18	0.35	0.35
Input voltage (V)	3–4.5	NA	2–4.5	2.6–6
Output voltage (V)	2.8	1.2	1.8	1.8
Dropout voltage (V)	0.199	0.2	0.2	0.125
Current efficiency (%)	NA	99.9	NA	99
Output current (mA)	150	200	200	0–200
Quiescent current (μA)	114	20	30	45
Current limit (mA)	NA	NA	NA	252
Line regulation (mV)	1.5	NA	6	4.5
Load regulation (mV)	17.4	NA	0.09	5
PSRR (dB)	67@20 K	45@20 K	NA	71@10 K
Thermal protection	No	No	No	Yes (<40 °C)

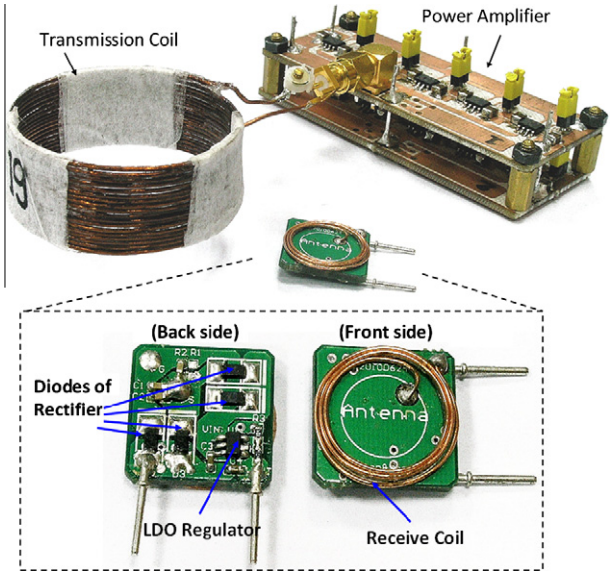

Fig. 10. Fabricated full system with power amplifier, transmission coil, receiving coil and LDO regulator.

tion. To generate the RF powering, a power amplifier module using commercial chips is used to amplify the 13.56 MHz signal from a signal generator. Fig. 10 shows the fabricated wireless powering system, the class-E power amplifier and receive module. Fig. 11 illustrates the temperature raise test under 37 °C environmental temperature, which is used to simulate the practical implant environmental condition with maximal output current (200 mA) for 1hr. Result shows that less than 2 °C raise is observed thus meet the implantation requirement [23,24].

Fig. 12 shows observation on the output performance of receive coil, rectifier and LDO chip by applying 13.56 M Hz signal to the Fig. 12A and B display the received power on receiving coil, the rectifier output and the LDO output when input signal on E-class amplifier is 2.5 V and 6.8 V, while related output current is 0 mA

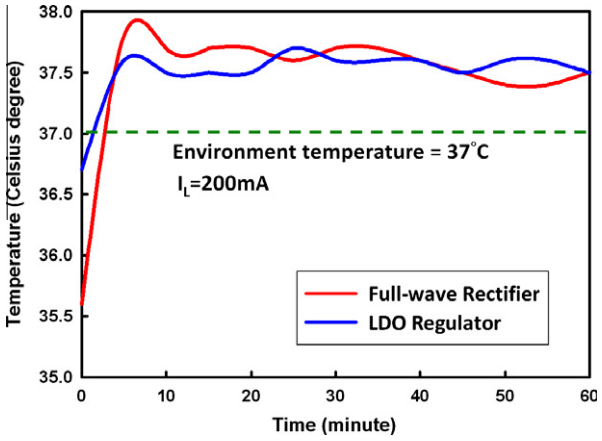

Fig. 11. Temperature raise test under 37 °C with maximal output current for 1hr.

and 200 mA, respectively. The maximal output ripple is around 50 mV due to the low PSRR performance at 13.56 M Hz. However, the ripple can be reduced down to less than 20 mV is extra 0.1 μF ceramic capacitance is added at the LDO output. Fig. 12C shows the Load Regulation under current loading varies from 100 mA to 200 mA. The Transient voltage is about 400 mV in peak. Table 3 shows the result of measured Load Regulation of the full system. Finally, the calculated specific absorption rate (SAR) is 0.27 W/kg, which is in the basic restriction of IEEE standard C95.1 (0.4 W/kg).

In ideal case, the quiescent current must be as low as possible during zero-to-low loading, because it amounts to a significant portion of the total drain current from the supply. However, in the other hand, the quiescent current of the circuit also determinates the response speed of the amplifier. Error amplifier compares the reference voltage between feedback voltage and operates the pass element for different loading condition. Low quiescent current can lead to slow response in pass element control. In this paper, the Load Regulation achieves 0.5 mV under the condition of 2.6 V input voltage, which is comparable to other systems. From the application point of view, the current load of an implant microsystem for neural signal recording is relative stable. Therefore, the quiescent current of our design can be reduced to small loading variation condition. Another possible method for improving the system is to apply additional buffer between error amplifier and the pass device. Under the condition of very low quiescent bias current amplifier design, the objective of the buffer is to drive the power pass device quickly with minimal power. The buffer must produce low output impedance because the large pass device presents large parasitic capacitance. Also, higher slew rate currents of the buffer is required to quickly charge and discharge the parasitic capacitance of pass device. Additionally, the buffer should exhibit high input impedance to decrease the loading effects in error amplifier, which may limit the loop gain and bandwidth of the regulator. Clearly, adding additional buffer may increase the complexity of the system. Related studies will be consider as our next steps.

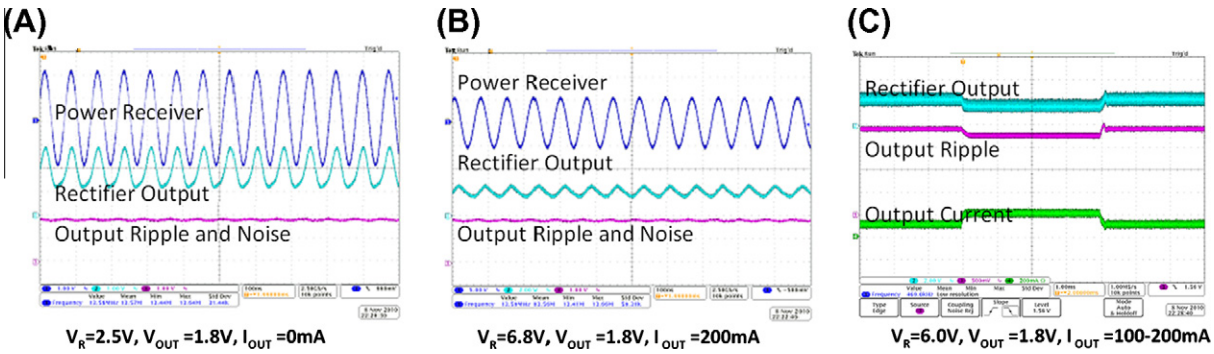

Fig. 12. (A) Output ripple observation under V_{IN} = 2.5 V, I_{OUT} = 0 mA (B) V_{IN} = 6.8 V, I_{OUT} = 200 mA (C) Load Regulation under I_{OUT} = 100–200 mA.

Table 3
Measured Load Regulation of the system.

Current	V_{OUT}
I_{OUT} = 0 mA	1.828 V
I_{OUT} = 50 mA	1.827 V
I_{OUT} = 100 mA	1.826 V
I_{OUT} = 150 mA	1.823 V
I_{OUT} = 200 mA	1.820 V
Load Regulation	8 mV

To summarize, the spiral coils as a wireless power module is presented in power management for batteryless medical instrumentation applications. The coil and circuit design, fabrication and system implementation are exhaustively discussed in this section. Finally, practical measurement result provides the detailed performance characterization of the presented wireless power module.

6. Conclusion

In this paper, we present a wireless RF-powering electronics approach for implantable biomedical applications on laboratory animals. Miniaturized spiral coils as a wireless power module with low-dropout linear regulator circuit convert RF signal into DC voltage, provide a batteryless implantation for truly free-behavior monitoring without wire dragging. Carefully designed inductive coupling coils provide wireless power transmission with 0.83 coupling coefficient and high antenna efficiency. The proposed LDO regulator achieves 45 μA quiescent-current, 4.5/5 mV Line/Load Regulation, 71 dB PSRR with thermal protection to avoid damage to the implanted tissue. The full system exhibits less than 20 mV ripple output and maximal 400 mV transient peak voltage under current load varies from 100 mA to 200 mA. Related system performance measurements have been successfully completed to demonstrate the wireless powering capabilities under safety issues considerations (temperature and SAR) in desired implantable microsystems.

Acknowledgements

This work was supported in part by Ministry of Economic Affairs, Taiwan, under Contract Number 98-EC-17-A-07-S1-011, and National Science Council, Taiwan, under Contract Number 99-2218-E-039-001, 99-2220-E-009-019, 99-2220-E-009-072, 99-2220-E-009-002 and in part by Taiwan Department of Health Clinical Trial and Research Center of Excellence under Contract Number DOH99-TD-B-111-004 and Number DOH99-TD-C-111-005. This work was supported in part by the UST-UCSD International Center of Excellence in Advanced Bio-engineering sponsored by the Taiwan National Science Council I-RiCE Program under Grant Number NSC-99-2911-I-009-101. The authors would like to thank National Chip Implementation Center (CIC) for chip fabrication.

References

[1] Young CP, Liang SF, Chang DW, Liao YC, Shaw FZ, Hsieh CH. A portable wireless online closed-loop seizure controller in freely moving rats. IEEE Trans Instrum Meas 2011;60:513–21.
[2] Deadwyler SA, Hampson RE, Collins V. A wireless recording system that utilizes Bluetooth technology to transmit neural activity in freely moving animals. J Neurosci Methods 2009;182:195–204.
[3] Denisov A, Yeatman E. Ultrasonic vs inductive power delivery for miniature biomedical implants. Body Sensor Networks (BSNs). In: International conference on 2010; 2010. p. 84–9.
[4] Chang CW, Chiou JC. Development of a three dimensional neural sensing device by a stacking method. Sensors-Basel 2010;10:4238–52.
[5] Towe BC, Larson PJ, Gulick DW. Wireless ultrasound-powered biotelemetry for implants. Engineering in medicine and biology society, 2009 EMBC 2009. In: Annual international conference of the IEEE; 2009. p. 5421–4.
[6] Sodagar AM, Amiri P. Capacitive coupling for power and data telemetry to implantable biomedical microsystems. I IEEE Embs C Neur E; 2009. 404–7.
[7] Zhu Y, Moheimani SOR, Yuce MR. Ultrasonic energy transmission and conversion using a 2-D MEMS resonator. IEEE Electron Device Lett 2010;31:374–6.
[8] Chang C-W, Hou K-C, Shieh L-J, Hung S-H, Chiou J-C. Wireless powering electronics and spiral coils for implant microsystem toward nanomedicine diagnosis and therapy in free-behavior animal. In: Nanoelectronics conference (INEC), 2011 IEEE 4th international; 2011. p. 1–2.
[9] Vaillancourt P, Djemouai A, Harvey JF, Sawan M. EM radiation behavior upon biological tissues in a radio-frequency power transfer link for a cortical visual implant. In: Proceedings of the 19th annual international conference of the IEEE engineering in medicine and biology society, vol. 19. Pts 1–6; 1997. p. 2499–502.
[10] Kendir GA, Liu WT, Wang GX, Sivaprakasam M, Bashirullah R, Humayun MS, et al. An optimal design methodology for inductive power link with class-E amplifier. IEEE Trans Circuits – I 2005;52:857–66.
[11] Jow UM, Ghovanloo M. Design and optimization of printed spiral coils for efficient transcutaneous inductive power transmission. IEEE Trans Biomed Circ S 2007;1:193–202.
[12] Poon ASY, O'Driscoll S, Meng TH. Optimal frequency for wireless power transmission into dispersive tissue. IEEE Trans Antenn Propag 2010;58:1739–50.
[13] Ko W, Liang S, Fung C. Design of radio-frequency powered coils for implant instruments. Med Biol Eng Comput 1977;15:634–40.
[14] Jow UM, Ghovanloo M. Modeling and optimization of printed spiral coils in air, saline, and muscle tissue environments. IEEE Trans Biomed Circ S 2009;3:339–47.
[15] Finkenzeller K. RFID handbook – fundamentals and applications in contactless smart cards and identification. 2nd ed. John Wiley & Sons; 2003.
[16] Harrison RR. Designing efficient inductive power links for implantable devices. IEEE Int Symp Circ S; 2007. p. 2080–3.
[17] Kurs A, Karalis A, Moffatt R, Joannopoulos JD, Fisher P, Soljacic M. Wireless power transfer via strongly coupled magnetic resonances. Science 2007;317:83–6.
[18] Rincon-Mora GA, Allen PE. A low-voltage, low quiescent current, low drop-out regulator. Solid-State Circuits, IEEE J 1998;33:36–44.
[19] Razavi B. Design of analog cmos integrated circuits; 2001.
[20] Wong K, Evans D. A 150 mA low noise, high PSRR low-dropout linear regulator in 0.13 mu m technology for RF SoC applications. Proc Eur Solid-State 2006:532–5.

[21] Liang-Guo S, Zu-Shu Y, Xing Z, Yuan-Fu Z, Ming G. A fast-response low-dropout regulator based on power-efficient low-voltage buffer. In: Circuits and systems, 2008 MWSCAS 2008 51st midwest, Symposium; 2008. p. 546–9.
[22] Chun-Yu H, Chih-Yu Y, Ke-Horng C. A low-dropout regulator with smooth peak current control topology for overcurrent protection. Power Electron, IEEE Trans 2010;25:1386–94.
[23] Wise KD, Sodagar AM, Yao Y, Gulari MN, Perlin GE, Najafi K. Microelectrodes, microelectronics, and implantable neural microsystems. P IEEE 2008;96:1184–202.
[24] Seese TM, Harasaki H, Saidel GM, Davies CR. Characterization of tissue morphology, angiogenesis, and temperature in the adaptive response of muscle tissue to chronic heating. Lab Invest 1998;78:1553–62.